AIRNet: Self-Supervised Affine Registration for 3D Medical Images using Neural Networks

Evelyn Chee
evelyn.chee@biomind.ai

Zhenzhou Wu
joe.wu@biomind.ai

Abstract

In this work, we propose a self-supervised learning method for affine image registration on 3D medical images. Unlike optimisation-based methods, our affine image registration network (AIRNet) is designed to directly estimate the transformation parameters between two input images without using any metric, which represents the quality of the registration, as the optimising function. But since it is costly to manually identify the transformation parameters between any two images, we leverage the abundance of cheap unlabelled data to generate a synthetic dataset for the training of the model. Additionally, the structure of AIRNet enables us to learn the discriminative features of the images which are useful for registration purpose. Our proposed method was evaluated on magnetic resonance images of the axial view of human brain and compared with the performance of a conventional image registration method. Experiments demonstrate that our approach achieves better overall performance on registration of images from different patients and modalities with 100x speed-up in execution time.

1 Introduction

Image registration [1] is the process of aligning different images into the same coordinate frame, enabling comparison or integration of images taken at different times, from different viewpoints, or by different sensors. It is used in many medical image analysis tasks. Several medical image registration studies have been conducted [2–5] and toolkits such as SimpleITK [6, 7], ANTs [8] and 3D Slicer [9] have been developed. Typically, registration processes implemented in those tools are performed by iteratively updating transformation parameters until a predefined metric, which measures the similarity of two images to be registered, is optimised. These conventional methods have been achieving decent performance, but their applications are limited by the slow registration speed. This is mainly because the iterative algorithm is optimising the cost function from scratch for every new registration task instead of utilising the information obtained from previous experiences.

To overcome this issue, many recent works done on medical image registration have proposed methods based on deep learning approaches, motivated by the successful applications of convolutional neural network (CNN) in the computer vision field. Wu et al. [10] use a convolutional stacked auto-encoder to learn the highly discriminative features of the images to be registered. However, the extracted features might not be optimal for registration purpose as the extraction is done separately for each image pairs. Also, the method proposed is not an end-to-end deep learning strategy as it still relies on other feature-based registration methods to find the mapping between the two images.

Subsequently, several works on end-to-end unsupervised registration using CNN have been presented. Similar to the conventional image registration methods, the strategy proposed by de

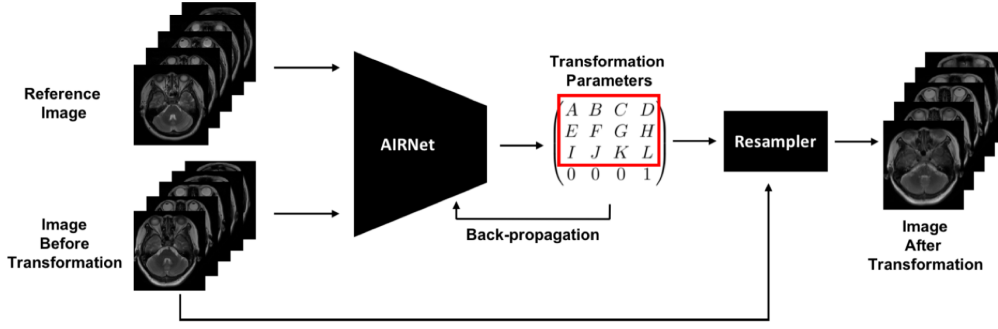arXiv:1810.02583v2 [cs.CV] 15 Oct 2018

Figure 1: The workflow of our image registration framework. The AIRNet takes two images and outputs the transformation parameters (*red box*). The image to be transformed is then warped by the resampler using the transformation matrix. During training, the loss function, which is the mean-squared error of the estimated transformation parameters, will be back-propagated to the network

Vos et al. [11] and Shan et al. [12] does not require any ground truth label on the image pairs to be registered. A predefined metric is used as the loss function and back-propagated to the CNNs to learn the optimal parameters of the network that minimises the error. This strategy is implementable by using the spatial transformer network introduced by Jaderberg et al. [13], which enables neural networks to spatially transform feature maps and is fully differentiable. To ensure the satisfactory performance of these frameworks, a good optimising metric must be defined. This could be a potential drawback as different metrics have their pros and cons and the suitability of a metric varies from task to task.

On the other hand, Miao et al. [14] use CNN regression to directly estimate the transformation parameters and there is no selection of the right optimising metric involved. The models were then trained on synthetic X-ray images as they provide ground truth labels without the need of manual annotation. Although higher registration success rates than conventional methods have been achieved, in their framework, six regressors were trained and applied in a hierarchical manner instead of estimating all the parameters simultaneously.

In this paper, we build a system (Fig. 1) for medical image registration, which also utilises CNN to calculate the transformation parameters between two 3D images. Unlike the unsupervised learning methods that maps the images to a scalar-valued metric function, our affine image registration network (AIRNet) requires two 3D images to be registered (input values) and the transformation parameters (target values). Here, we use a twelve-dimensional vector capturing 3D affine transformation as the label of each input data. But since it is impractical to manually identify the transformation parameters between any two images, we explore a self-supervised learning method and leverage the abundance of cheap unlabelled data to generate a synthetic dataset for the training of the model. Through direct estimation of transformation matrix, our method performs one-shot registration instead of hierarchical manner as presented by Miao et al [14].

Furthermore, the structure of the AIRNet enables us to learn the discriminative features of the images which are useful for registration purpose. Additionally, the features allow us to obtain generalised representations of different image modalities. For instance, different set of a brain scan can be generated based on different settings of magnetic resonance (MR) brain imaging protocol, rendering the intensity of the brain tissue to differ across modalities. But for brain volumes which are aligned, the representation of these images would be similar as the registration

focuses on geometric information.

In short, we develop a deep learning framework for 3D image registration which achieves better overall performance at 100x faster speed in execution as compared to some conventional methods. Our framework is applicable for two main areas in medical imaging: 1) registration of images from different patients to identify different anatomical regions of the body, and 2) registration of images from different modalities to integrate useful information across different type of data. The rest of the paper is organised as follows: Sect. 2 defines our problem; Sect. 3 introduces our proposed method; Sect. 4 presents the experimental results.

2   Problem Statement

In this paper, the image registration system focuses on 3D affine transformation, which includes translation, scaling, rotation and shearing. Each of these transformation can be parameterised by a matrix T as shown in Fig. 1. Using these matrices, we map an input coordinate to another coordinate and obtain the desired transformation effect. In other words, for any pixel coordinates $\vec{x}$ in a 3D image, the new pixel location can be computed by $\vec{x}' = T\vec{x}$. The values of the unknowns in the matrix indicate the amount of translation, scaling, rotation and shearing. Replacing these letters by different values would lead to various compositions of these transformations. Hence, it is sufficient to represent the relationship between two 3D images using a twelve-dimensional vector $\vec{t}$, which is the flatten copy of the top three rows of matrix T.

As shown in Fig. 1, the inputs of our framework are the two images to be registered. We denote the reference image as I_{ref} and the other image to be shifted to match the reference as $I_{\vec{t}}$, where $\vec{t}$ is the unknown ground truth transformation parameters. The registration problem is then formulated as

$$\vec{t} = \text{AIRNet}(I_{ref}, I_{\vec{t}}), \tag{1}$$

where the AIRNet is trained to find the mapping from the input images to the transformation parameters. The design of the network and methods used to find the optimal weights in the AIRNet will be discussed in the next section.

3   Methods

This section describes the architecture of the AIRNet and the training procedure.

3.1   Network Architecture

The AIRNet is designed to model the affine transformation relationship between two input images as shown in Fig 2. There are two main components in the network: the encoder part which captures discriminative features of the input images and the regression part which finds the non-linear relationship between the features and the corresponding transformation parameters.

For the encoder, it learns a new representation of the input data optimally for registration purpose, and these representations allow us to gain insights to the image dataset. From Fig. 2, the encoder is composed of two pathways, one for each input image. The corresponding blocks from both pathways share the same parameters. Weight sharing between blocks allows us to learn the same encoder for feature extraction of both images, as well as reduces the number of parameters in the first part of the network by half to minimise the risk of overfitting.

The architecture of the encoder is adapted from DenseNet [15], in which the building blocks have skip connections to allow integration of high and low-level feature information. An additional property of our network is the mixture of 2D and 3D filters which aims to resolve the
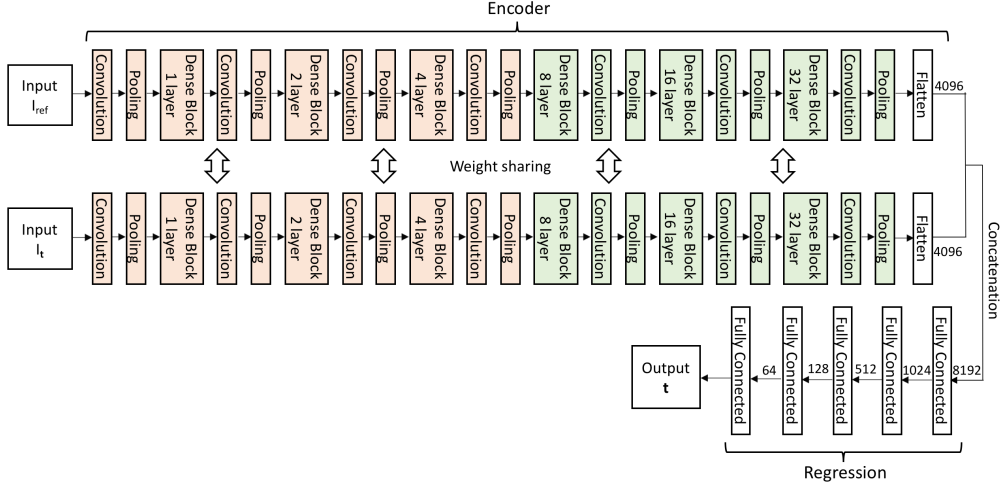
Figure 2: Architecture of AIRNet. Two separate paths are used for I_{ref} and $I_{\vec{t}}$. The layers before concatenation act as an encoder to learn representations of the data and each block from the two pathways share the same parameters. The first part of the encoder (*orange blocks*) consists of 2D filters whereas 3D filters are used in the remaining part (*green blocks*). The outputs of the encoder are flatten and concatenated before passed into the fully connected layers

anisotropicity of the 3D medical images, i.e. the depth of the input image is much smaller compared to its height and width. So, in the initial part of the encoder, 2D filters are used in the convolutional and pooling layers. The height and width of the feature maps are shrunk as the effect of the 2D pooling layers. Consequently, the size of the features in the height and width directions will eventually be similar to that in the depth direction, after which 3D convolutional and pooling layers will be used.

Each input image firstly undergoes a 3×3 convolutional layer and is downsized using a 2×2 max-pooling layer. The dense blocks are made of multiple 2D (resp., 3D) convolutional layers with a growth rate of 8 with each layer taking the input of the previous feature map as input. The number of layers in each dense block are indicated in Fig. 2. More layers are added as the network goes deeper because deeper layers generally correspond to more specific features and hence, require more channels to capture. Next, the transition layers, which are the layers between dense blocks, consist of an 1×1 (resp., $1 \times 1 \times 1$) convolutional layer, a batch normalisation layer and a Rectified Linear Unit (ReLU) function followed by a 2×2 (resp., $2 \times 2 \times 2$) max-pooling layer with a stride of 2.

The outputs of both flatting layers are then concatenated and given as input to the regression part. The fully connected layers are where the high-level reasoning is done and the non-linear relationship between features extracted from the encoder is decided. These layers consist of linear layers, batch normalisation layers and ReLU functions. The regression model will then return the transformation parameters that align the input images.

3.2   Training

Our proposed framework is experimented on with MR images of the axial view of human brain from our hospital database and we trained the network in a supervised manner by minimising a loss between the actual and predicted transformation parameters. However, information regard-
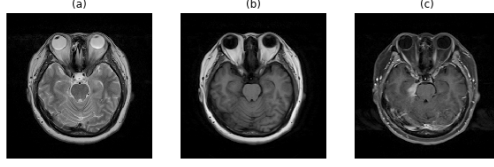
4

Figure 3: MR brain images in the axial plane which are: (a) T2-weighted, (b) T1-weighted, (c) contrast-enhanced T1-weighted

ing the transformation matrix between any two of the images are not available. Thus, we used a self-supervised learning approach and trained the network on synthetic MR images. The process of generating this training dataset should provide reliable ground truth labels with little manual annotation. So, for every brain scan, a random transformation matrix T was generated. The range of each transformation type could be set according to the aim of each particular experiment. In our case, the constraints of the parameters are as follows (x, y and z-axis corresponds to the width, height and depth direction): angle of rotation about z-axis ranges from -0.8 to 0.8 radians; translation ranges from -0.15 to 0.15 along x and y-axis and -0.2 to 0.2 along z-axis; scaling across all axes ranges from 0.8 to 1.3. The matrix T was then applied onto the image to produce an affine transformed version of the brain scan. These two images are now the two input images of the network, $I_{\vec{t}}$ and I_{ref} respectively where the ground truth label of the input pair, $\vec{t}$, is the flatten copy of the top three rows of matrix T.

There are some pre-processing methods implemented on the images. Firstly, to ensure performance, the range of pixel values in different input images is unified by normalising the pixel values to a range between zero and one. Secondly, the images were resized and resampled so that all images have the same dimension, which in this case is $20 \times 320 \times 320$ pixels.

As introduced earlier, the encoder in the AIRNet is able to extract a generalised representation of different image modalities. Three modalities used in this study are T2-weighted, T1-weighted and contrast-enhanced T1-weighted (Fig. 3). Although pixel intensities of the same brain tissue can vary in different modalities, the encoder can capture general features across modalities. The selection of most discriminative features, which concisely describe complex morphological patterns of the brain, addresses the concern of the registration method not being able to scale well to various image modalities. To test the effectiveness of our encoder, three training datasets were prepared:

- $S_{1,2,c}$: All three modalities are included in the dataset and each image pair, I_{ref} and $I_{\vec{t}}$ are of the same modality.

- $S_{1,2}$: Each image pair are of the same modality but only images of T2 and T1-weighted are used.

- $D_{1,2}$: For each patient, images of T2 and T1-weighted are already aligned because both are acquired through one scan and hence, we constructed a dataset which have these two different modalities within each image pair.

Using these datasets, we trained three models using Tensorflow [16]. The objective function to be minimised during the training is defined as:

$$Loss = \frac{1}{K} \sum_{i=1}^{K} ||\vec{t}^{[i]} - \text{AIRNet}(I_{ref^{[i]}}, I_{\vec{t}^{[i]}}; \vec{W})||_2^2, \tag{2}$$

5

where K is the number of training sample, $\vec{W}$ is a vector of weights in the network that needs to be learned, $I_{ref[i]}$ and $I_{\vec{t}[i]}$ are the i-th training input pairs, $\vec{t}^{[i]}$ is the label of the i-th training sample, $\text{AIRNet}(I_{ref[i]}, I_{\vec{t}[i]}; \vec{W})$ is the output of the network parameterised by $\vec{W}$ on the i-th training sample. The weights $\vec{W}$ are learned using the Adam optimiser algorithm [17].

4   Experiments and Results

As described in the previous section, the AIRNet estimates the transformation matrix given two images. This matrix is then feed into a resampler which wraps one of the image to the other. Later, registration performance of the trained neural network will be assessed and compared with a conventional registration method.

4.1   Conventional Registration Algorithm

The conventional registration method we used is the affine transformation function available under the SimpleITK [6, 7] registration framework. Mattes mutual information [18] with the default settings is selected as the similarity metric and linear interpolator is used. For the optimiser, we adopted regular step gradient descent with learning rate of 0.005, minimum step of 1×10^{-10} and number of iterations as 10000.

4.2   Evaluation

We evaluate the trained models on a MR brain image dataset with ground truth segmentation masks which were prepared from our hospital database. This dataset consists of twelve subjects and each has T2 and T1-weighted MR images. For each subject, manual anatomical segmentation of the brain has been done. Since the image of both modalities are aligned, the segmentation masks are applicable to both images.

For any two images which are perfectly registered, the brain parts represented by matching pixels should be consistent in both images. Hence, we could use the similarity between the segmentation masks of the reference and registered images to evaluate the performance of the registration methods. The following metrics are used throughout all experiments to compare two masks, A and B:

- Jaccard index (Jac): It is used for measuring the similarity of the masks and is defined as the size of their intersection divided by the size of their union:

$$Jac(A, B) = \frac{|A \cap B|}{|A \cup B|}. \tag{3}$$

- Modified Hausdorff distance [19] (d_H): It measures the distance between two masks and is defined as the average of all the distances from a boundary point in one mask to the closest boundary point in the other mask:

$$d_H(A, B) = \max\{\frac{1}{|P_A|} \sum_{a \in P_A} \inf_{b \in P_B} d(a, b), \frac{1}{|P_B|} \sum_{b \in P_B} \inf_{a \in P_A} d(a, b)\}, \tag{4}$$

where P_A and P_B are the set of boundary points in A and B respectively, d represents the Euclidean distance, and $|\cdot|$ measures the number of elements in the set.

The third metric reported is the running time, which records the total time required, in seconds, to calculate the transformation parameters of the two images. The results indicated are based on the implementation of the algorithms on a Intel Xeon CPU E5-2630 v4 2.2GHz.

Table 1: Performance of the conventional methods and our proposed framework when evaluated on the temporal lobe. The metrics are 1) mean Jaccard index across all subjects, 2) mean modified Hausdorff distance across all subjects, and 3) average and standard deviation of running time per registration. For the two respective experiments, the rows list results before registration, with registration using SimpleITK, and results obtained using our three trained models. The best results are highlighted in bold.

Experiment	Method	Jac	d_H	Running Time
-	No registration	0.491	2.270	-
E_p	SimpleITK [6,7]	0.561	1.876	166.537±89.844
	AIRNet-$S_{1,2,c}$	**0.613**	**1.431**	0.785±0.027
	AIRNet-$S_{1,2}$	0.586	1.546	0.778±0.036
	AIRNet-$D_{1,2}$	0.599	1.512	0738±0.016
$E_{p,m}$	SimpleITK [6,7]	0.524	1.978	216.848±114.369
	AIRNet-$S_{1,2,c}$	**0.615**	**1.459**	0.793±0.034
	AIRNet-$S_{1,2}$	0.577	1.574	0.772±0.028
	AIRNet-$D_{1,2}$	0.601	1.475	0.755±0.022

4.3   Registration Results

We firstly select one subject P from the test dataset to act as a reference point. In other words, the MR images of this subject will be used as I_{ref} in the following two experiments:

- E_p (across patients registration): Registering T1-weighted image of the remaining subjects to T1-weighted image of subject P;

- $E_{p,m}$ (across patients and modalities registration): Registering T1-weighted image of the remaining subjects to T2-weighted image of subject P.

The estimated transformation parameters are then fed into the resampler to wrap the corresponding segmentation masks. We firstly evaluate the metrics on the segmentation mask of one particular brain part, which is the temporal lobe and the performance of our neural registration models and the conventional method are shown in Table 1. Our proposed models have relatively constant execution speed and are 100x faster than the conventional method. At the same time, they still achieve better overall registration performance for this region. Fig. 4 illustrates an example of the registration results from experiment $E_{p,m}$.

Next, we evaluate the performance of the methods on ten out of the eighteen brain regions which are labelled. We note that in some methods, only affine transformation is involved and hence, not all of the brain parts will be registered perfectly. The registration performance could vary across different brain regions and the results are shown in Fig. 5 and Table 2.

On the whole, it is observed that except for AIRNet-$D_{1,2}$, all other methods perform better in across patients registration, E_p. In fact, the conventional algorithm displays the most significant improvement in terms of the metric values, suggesting that it is more favourable for registration tasks on images of the same modality. As opposed to the other models, AIRNet-$D_{1,2}$ was trained on image pairs of different modalities, and hence is reasonable to perform better in $E_{p,m}$. However, when compared with AIRNet-$S_{1,2,c}$, there was only a slight advantage in performance. Our framework using AIRNet-$S_{1,2,c}$ is still the overall best and has achieved better results in
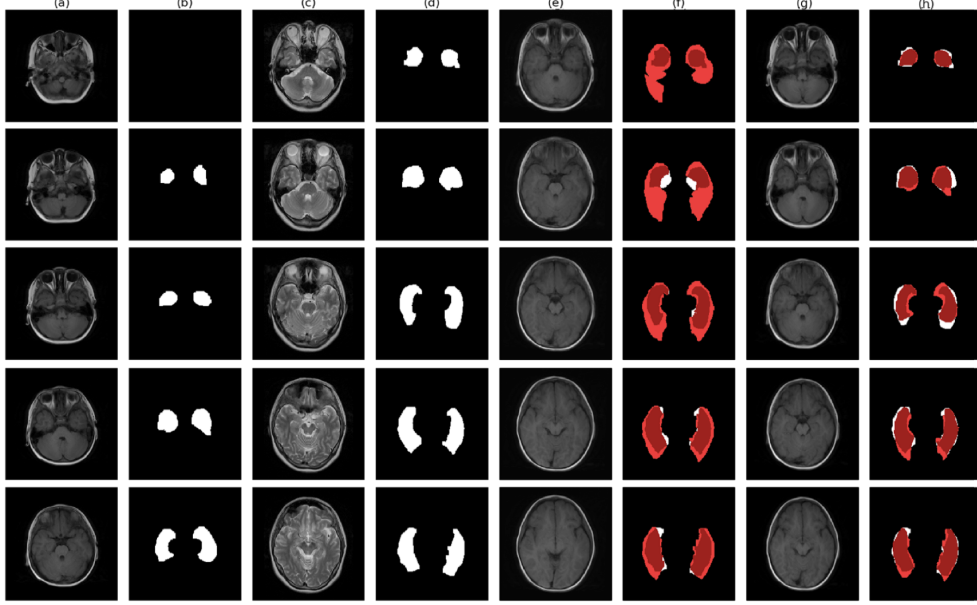
Figure 4: Illustration of the brain registration performance of AIRNet-$S_{1,2,c}$ and the conventional registration algorithm. The snapshots shown are slice 5 to 9 of the following: (a) Image to be registered $I_{\vec{t}}$; (b) Ground truth segmentation mask of $I_{\vec{t}}$; (c) Reference image I_{ref}; (d) Ground truth segmentation mask of I_{ref}. (e) and (g) are $I_{\vec{t}}$ warped by SimpleITK and AIRNet respectively. The red masks in (f) and (h) are the warped ground truth segmentation mask which corresponds to (e) and (g) while the white masks are the ground truth segmentation mask of I_{ref}

Table 2: Average performance of the conventional methods and our proposed framework summarised from Fig. 5. [left] Average percentage improvement in the metrics across ten brain parts when compared to before registration. [right] Number of regions which our proposed method performs better than the conventional method in terms of the respective metrics. The best results are highlighted in bold.

Method	E_p		$E_{p,m}$	
	Jac	d_H	Jac	d_H
SimpleITK [6,7]	25.5	23.8	17.6	19.6
AIRNet-$S_{1,2,c}$	**28.6**	**39.8**	24.5	**37.5**
AIRNet-$S_{1,2}$	19.4	32.3	15.9	30.7
AIRNet-$D_{1,2}$	21.9	34.6	**24.6**	37.2

Method	E_p		$E_{p,m}$	
	Jac	d_H	Jac	d_H
AIRNet-$S_{1,2,c}$	**5**	**10**	7	**10**
AIRNet-$S_{1,2}$	4	7	6	8
AIRNet-$D_{1,2}$	3	9	**8**	**10**

(a) Percentage Change in Metric Values on 10 Brain Regions After Registration in E_p

(b) Percentage Change in Metric Values on 10 Brain Regions After Registration in $E_{p,m}$

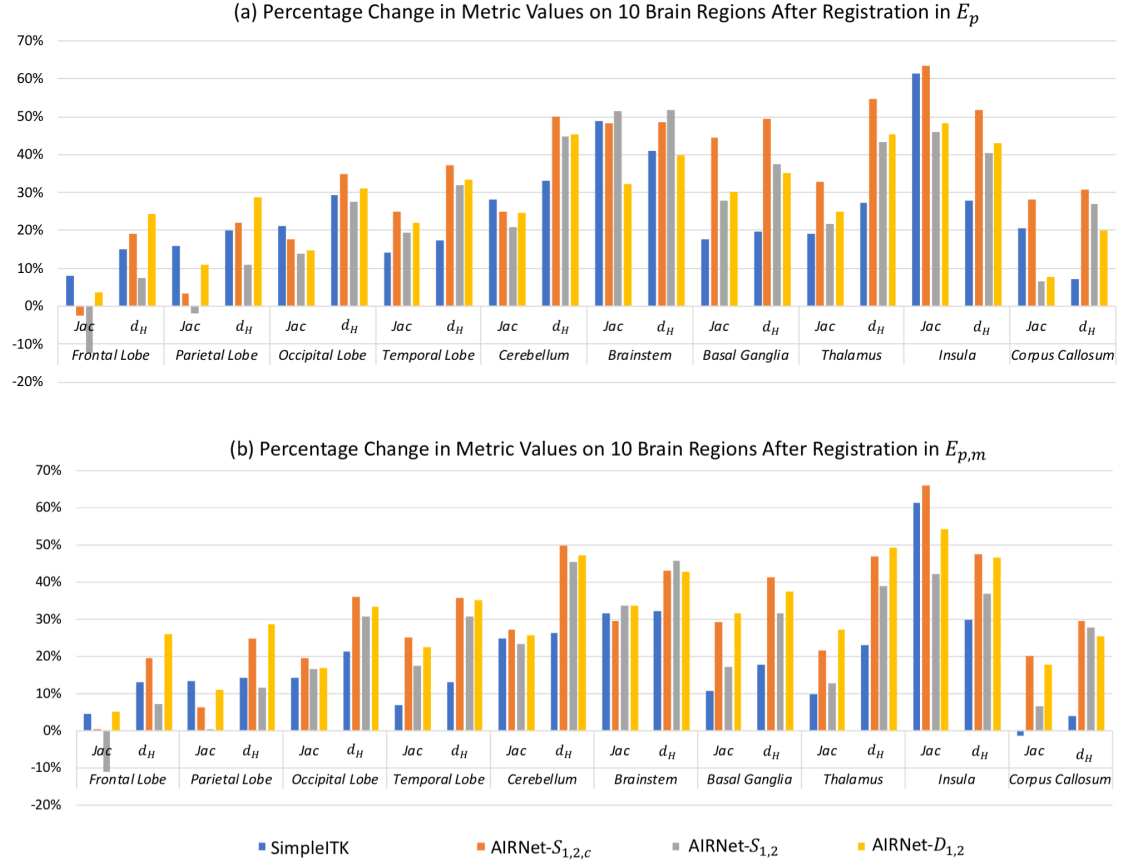SimpleITK   AIRNet-$S_{1,2,c}$ AIRNet-$S_{1,2}$ AIRNet-$D_{1,2}$

Figure 5: Performance of the conventional method and our models when evaluated on ten regions of the brain. The charts show the percentage change in the mean Jaccard index and modified Hausdorff distance on each region when compared to before registration

majority of the ten brain regions. This self-supervised learning method would be preferable because during the dataset preparation, it only requires one image for each training sample instead of two aligned images of different modalities. In addition, it is more flexible in terms of the number of modalities that can be included. Lastly, we observe that even though T1-weighted MR images were not included in the training of AIRNet-$S_{1,2}$, it still manages to perform reasonably well on the test cases which involve this image modality, indicating that the network is able to recover the same features from the unseen data type.

To summarise, our proposed framework based on self-supervised learning can register images significantly faster than the conventional method and can achieve superior performance both in terms of Jac and d_H. Although trained on image pairs of the same patient and modality, the model still works well on images without such properties. Thus, our method can be applied to registration of images from different patients and/or modalities. The AIRNet also provides decent registration results when tested on images of unseen modalities, indicating that the network encoder is extracting generalised features of the image regardless of its modality. We visualise and further verify this inference in the next part.

4.4 Encoder Output Visualisation

In this part, we examined the output of the encoder of our best performing model AIRNet-$S_{1,2,c}$. For each input image, we extract the output of the flattening layer in the network, which would be the new representation of this image. To visualise this high dimensional output, we use principal component analysis (PCA) [20,21] and t-Distributed Stochastic Neighbour Embedding (t-SNE) [22].

First, the representation of MR images with the brains being rotated at various angles were extracted and visualised in the first image of Fig. 6. Samples are clustered according to their rotation angle, indicating that the encoder is able to incorporate information regarding the angle of rotation for each image. Although T2 and contrast-enhanced T1-weighted images are included, there is no significant boundaries between modalities, emphasising that the encoded representation are classified mainly based on the transformation instead of modality. This suggests that the encoder views the same brain scan of different modalities similarly and focuses on extracting geometric information. Similarly, the second image in Fig. 6 visualises the clusters of the encoder output based on the amount of shift applied onto the images. The samples of different modalities are not labelled explicitly but there is also no obvious boundary between them as observed previously.

Additionally, we visualise the trajectory of the registration results of our proposed method and the conventional algorithm. Fig. 7 shows an example of such visualisation illustrating the images before and after registration on the eleven subjects from $E_{p,m}$. All images were passed through the encoder to obtain their representation. For both methods, the registered images are more clustered and have moved towards the reference image in terms of PCA dimensions. Moreover, it is observed that the results from our proposed framework are closer to the target, agreeing with the performance shown in Table 2.

Taken together, the results suggest that the encoder is useful in selecting discriminative features that describe complex patterns in the images and provide important information to perform the image registration task.

5 Conclusions

A self-supervised learning method for affine 3D image registration has been presented and evaluated on medical images, specifically on axial view of brain scans. The presented system achieves
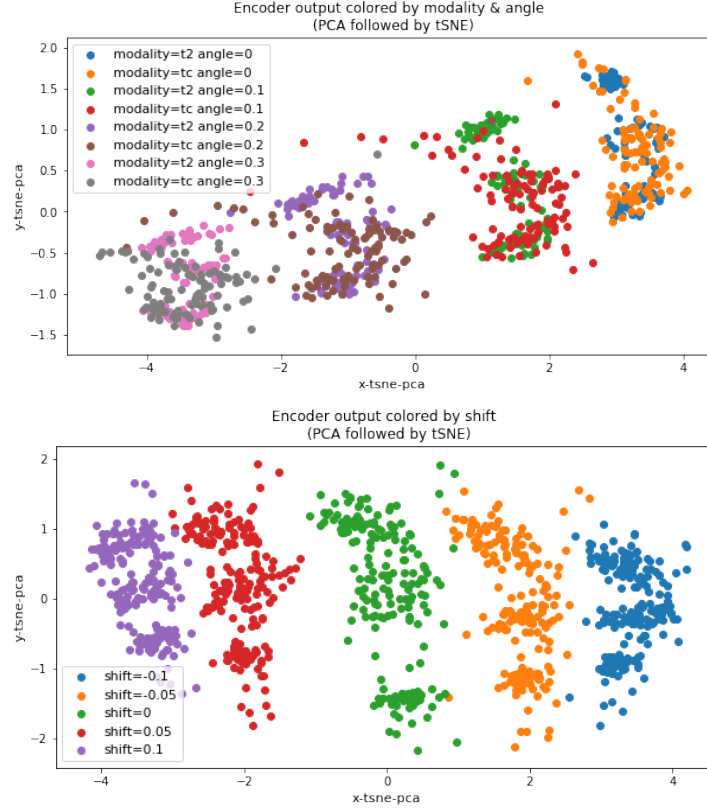
Figure 6: Scatter plot of encoder outputs after dimensionality-reduction using PCA, followed by tSNE. [above] Each sample is labeled by the angle (in radians) that it is rotated and the type of modality ($t2$ is T2-weighted and tc is contrast-enhanced T1-weighted). [below] Each sample is categorised by the type of translation used
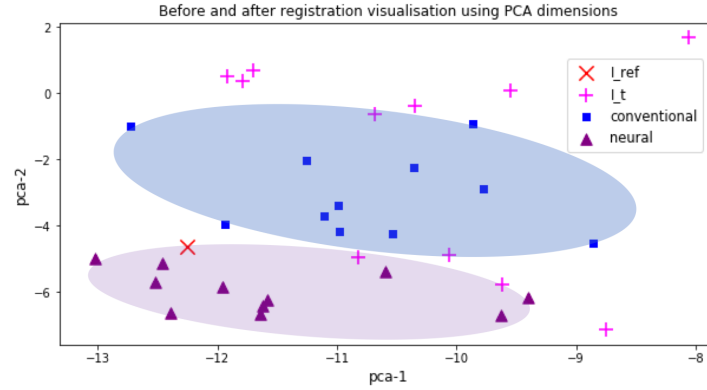

Figure 7: Scatter plot of encoder outputs of images from $E_{p,m}$ after dimensionality-reduction using PCA. The red and pink markers represent the reference image I_{ref} and images to be registered $I_{\vec{t}}$ respectively. The registration results using AIRNet-$S_{1,2,c}$ and SimpleITK are indicated by the purple and blue markers

a superior performance compared to a conventional image registration method at a much shorter execution time.

Since it is time-consuming and tedious to obtain information regarding the transformation between every two 3D images, we created a synthetic dataset using the existing medical images so that for each images, we have a new transformed image and a label for the pair without the need of manual annotation. With these data, we proceed with the training of the AIRNet in a self-supervised manner. Although each input pair of the training data are of the same patient and same modality, the trained network were tested for registration across patients and modalities and it still manages to perform well as compared with the conventional method.

Besides having a network which is able to find an affine transformation between two images, the way the AIRNet is constructed enables us to find a good feature representation of the images. This representation provides a concise description of the complex morphological patterns of the images regardless of the modality of the input images.

To sum up, our experiments show good registration results for images between different patients and different modalities by extracting useful features of the input images. To extend the applicability of the proposed method in future work, performing deformable registration will be investigated. Moreover, experiments were performed using only axial view of brain scans, but this can be extended to register any other type of 3D images.

References

[1] B. Zitov and J. Flusser. Image registration methods: a survey. *Image & Vision Computing*, 21(11):977–1000, 2003.

[2] J. Maintz and M. A. Viergever. A survey of medical image registration. *Medical Image Analysis*, 2:1–36, 1998.

[3] H. Lester and S. R. Arridge. A survey of hierarchical non-linear medical image registration. *Pattern Recognition*, 32(1):129–149, 1998.

[4] D. L. G. Hill, P. G. Batchelor, Holden M., and D. J. Hawkes. Medical image registration. *Physics in Medicine & Biology*, 46, 2001.

[5] J. P. W. Pluim, J. B. A. Maintz, and M. A. Viergever. Mutual-information-based registration of medical images: a survey. *IEEE Transactions on Medical Imaging*, 22(8):986–1004, 2003.

[6] B. C. Lowekamp, D. Chen, I. Luis, and B. Daniel. The design of simpleitk. *Frontiers in Neuroinformatics*, 7(7):45, 2013.

[7] Z. Yaniv, B. C. Lowekamp, H. J. Johnson, and R. Beare. Simpleitk image-analysis notebooks: a collaborative environment for education and reproducible research. *Journal of Digital Imaging*, 31(3):1–14, 2017.

[8] B. B. Avants, N. J. Tustison, G. Song, P. A. Cook, A. Klein, and J. C. Gee. A reproducible evaluation of ants similarity metric performance in brain image registration. *Neuroimage*, 54(3):2033–2044, 2011.

[9] A. Fedorov, R. Beichel, J. Kalpathy-Cramer, J. Finet, J. C. Fillion-Robin, S. Pujol, C. Bauer, D. Jennings, F. Fennessy, and M. Sonka. 3d slicer as an image computing platform for the quantitative imaging network. *Magnetic Resonance Imaging*, 30(9):1323–1341, 2012.

[10] G. Wu, M. Kim, Q. Wang, B. C. Munsell, and D. Shen. Scalable high performance image registration framework by unsupervised deep feature representations learning. *IEEE Transactions on Biomedical Engineering*, 63:1505–1516, 2016.

[11] B. D. D. Vos, F. F. Berendsen, M. A. Viergever, M. Staring, and I. Igum. End-to-end unsupervised deformable image registration with a convolutional neural network. In *Deep Learning in Medical Image Analysis and Multimodal Learning for Clinical Decision Support*, pages 204–212, 2017.

[12] S. Shan, X. Guo, W. Yan, E. I. Chang, Y. Fan, and Y. Xu. Unsupervised end-to-end learning for deformable medical image registration. 2018.

[13] M. Jaderberg, K. Simonyan, A. Zisserman, and K. Kavukcuoglu. Spatial transformer networks. *Advances in Neural Information Processing Systems*, 28:2017–2025, 2015.

[14] S. Miao, Z. J. Wang, Y. Zheng, and R. Liao. Real-time 2d/3d registration via cnn regression. In *IEEE International Symposium on Biomedical Imaging*, pages 636–648, 2016.

[15] G. Huang, Z. Liu, L. V. D. Maaten, and K. Q. Weinberger. Densely connected convolutional networks. In *IEEE Conference on Computer Vision and Pattern Recognition*, pages 2261–2269, 2017.

[16] M. Abadi, A. Agarwal, P. Barham, E. Brevdo, Z. Chen, C. Citro, G. S. Corrado, A. Davis, J. Dean, and M. Devin. Tensorflow: Large-scale machine learning on heterogeneous distributed systems. 2016.

[17] D. P. Kingma and J. Ba. Adam: A method for stochastic optimization. *Computer Science*, 2014.

[18] D. Mattes, D. R. Haynor, H. Veselle, T. K. Lewellyn, and W. Eubank. Nonrigid multimodality image registration. In *Proceedings of SPIE*, volume 4322, pages 4322–4322–12, 2001.

[19] M. P. Dubuisson and A. K. Jain. A modified hausdorff distance for object matching. In *International Conference on Pattern Recognition*, pages 566–568 vol.1, 2002.

[20] K. Pearson. On lines and planes of closest fit to systems of points in space. *Philosophical Magazine*, 2:559–572, 1901.

[21] H. Hotelling. Analysis of a complex of statistical variables with principal components. *Journal of Educational Psychology*, 24:417–441, 1933.

[22] G. E. Hinton. Visualizing high-dimensional data using t-sne. *Journal of Machine Learning Research*, 9(2):2579–2605, 2008.